Applied Surface Science 333 (2015) 59–67

Contents lists available at ScienceDirect

Applied Surface Science

journal homepage: www.elsevier.com/locate/apsusc

Experimental study on Hg^0 removal from flue gas over columnar MnO_x-CeO_2/activated coke

Yine Xie[a,b], Caiting Li[a,b,*], Lingkui Zhao[a,b], Jie Zhang[a,b], Guangming Zeng[a,b], Xunan Zhang[a,b], Wei Zhang[a,b], Shasha Tao[a,b]

[a] College of Environmental Science and Engineering, Hunan University, Changsha 410082, PR China
[b] Key Laboratory of Environmental Biology and Pollution Control, Hunan University, Ministry of Education, Changsha 410082, PR China

ARTICLE INFO

Article history:
Received 18 November 2014
Received in revised form 21 January 2015
Accepted 31 January 2015
Available online 7 February 2015

Keywords:
Elemental mercury
Activated coke
Adsorption
Catalytic oxidation
Flue gas

ABSTRACT

Mn-Ce mixed oxides supported on commercial columnar activated coke (MnCe/AC) were employed to remove elemental mercury (Hg^0) at low temperatures (100–250 °C) without the assistance of HCl in flue gas. The samples were characterized by X-ray diffraction (XRD), Brunauer–Emmett–Teller (BET), X-ray photoelectron spectroscopy (XPS) and temperature programmed desorption (TPD). Effects of some factors, including Mn-Ce loading values, active component, reaction temperatures and flue gas components (O_2, SO_2, NO, H_2O), on Hg^0 removal efficiency were investigated. Results indicated that the optimal Mn-Ce loading value and reaction temperature were 6% and 190 °C, respectively. Considerable high Hg^0 removal efficiency (>90%) can be obtained over MnCe6/AC under both N_2/O_2 atmosphere and simulated flue gas atmosphere at 190 °C. Besides, it was observed that O_2 and NO exerted a promotional effect on Hg^0 removal, H_2O exhibited a suppressive effect, and SO_2 hindered Hg^0 removal seriously when in the absence of O_2. Furthermore, the XPS spectra of Hg 4f and Hg-TPD results showed that the captured mercury were existed as Hg^0 and HgO on the MnCe6/AC, and HgO was the major species, which illustrated that adsorption and catalytic oxidation process were included for Hg^0 removal over MnCe6/AC, and catalytic oxidation played the critical role. What's more, both lattice oxygen and chemisorbed oxygen or OH groups on MnCe6/AC contributed to Hg^0 oxidation. MnCe6/AC, which exhibited excellent performance on Hg^0 removal in the absence of HCl, appeared to be promising in industrial application, especially for low-rank coal fired flue gas.

1. Introduction

Mercury, as a hazardous and toxic pollutant, has received a large number of attention around the world because of its high toxicity, volatility, persistence and bioaccumulation in the environment [1,2]. Among various sources of mercury emission, coal-fired utility boilers were reported to be the largest anthropogenic source in the United States, which account for approximately one-third of mercury emissions [3]. On December 16, 2011, the U.S. Environmental Protection Agency (EPA) promulgated a federal Mercury and Air Toxics Standards to limit mercury and other toxic air pollutions from power plants. The federal emission standards for mercury is to prevent about 90% of mercury in coal burned in power plants from being released to the air [4]. Therefore, researching and developing feasible mercury control technologies is required so as to meet the stringent standards.

The efficiency of mercury removal greatly depends on the forms of mercury. Generally, mercury in coal-fired flue gas is in three forms, namely elemental mercury (Hg^0), oxidized mercury (Hg^{2+}) and particulate-bound mercury (Hg^p) [5]. Among them, Hg^{2+} tends to be soluble in water, which can be removed by wet flue gas desulfurization equipments [6,7], and Hg^p can be captured by electrostatic precipitators or bag filters along with fly ash particles [8,9]. However, Hg^0 is difficult to be removed on account of its highly volatility and nearly insoluble in water, which becomes the biggest obstacle for mercury control.

Up to now, a number of methods, mainly including catalytic oxidation [10–12] and adsorption [13–15], have been developed to reduce Hg^0 emission. Thereinto, activated carbon injection (ACI), which has been applied in some coal-fired power plants [13], is the most mature technology for mercury removal [1,16]. However, it is restricted in widespread application for its drawbacks, such

* Corresponding author at: College of Environmental Science and Engineering, Hunan University, Changsha 410082, PR China. Tel.: +86 731 88649216; fax: +86 731 88649216.
E-mail addresses: ctli@hnu.edu.cn, ctli3@yahoo.com (C. Li).

http://dx.doi.org/10.1016/j.apsusc.2015.01.234
0169-4332/

as high cost, low utilization rate, inaccessible for sorbent recovery and its negative effect on the usage of fly ash [17–19]. Accordingly, various catalysts for catalytic oxidation of Hg^0 to Hg^{2+} were developed in recent years, especially some single metal oxides or binary metal oxides supported on different carries, such as MnO_x/Al_2O_3 [20], CeO_2-TiO_2 [21], CuO/TiO_2 [22], CeO_2-WO_3/TiO_2 [23], CuO-MnO_2-Fe_2O_3/γ-Al_2O_3 [11], SiO_2-TiO_2-V_2O_5 [24], V_2O_5-WO_3/TiO_2 [25]. However, the Hg^0 oxidation efficiency over some of these catalysts largely depends on the content of HCl in flue gas, so they were not good choices for treating flue gas derived from low-rank coal combustion. Therefore, developing a catalyst and/or adsorbent that could remove mercury effectively without the assistance of HCl is of tremendous value.

Activated coke (AC), as an adsorbent and catalyst, has been reported to be active for removing SO_2 and NO from flue gas simultaneously [26,27]. A successful practical application is the Mitsui-BF process [28], which uses coal-derived activated coke as a catalyst and adsorbent for SO_2 and NO removal. Moreover, taking industrial application into consideration, the activated coke owns several advantages. Firstly, it can resist crushing and abrasion effectively because of its great mechanical strength. Secondly, activated coke in granular form is suitable to be used in both moving bed and fixed bed unit. Thirdly, activated coke could be regenerated and the price is lower in comparison with powder activated carbon. Last but not the least, activated coke possesses a relative high surface area and various functional groups, which could provide the active sites for the physical and chemical adsorption of elemental mercury. Consequently, it is a promising candidate adsorbent and catalyst for Hg^0 removal in industry.

To improve the mercury removal capacity, some researchers tried to modify activated coke using various methods. For instance, activated coke impregnated with V_2O_5 [29], CeO_2 [30], $CeCl_3$ [31] were used to remove mercury from simulated flue gas in recent studies, which displayed higher mercury removal efficacy in comparison with virgin activated coke. Over the past few years, MnO_x-CeO_2 mixed oxides supported on various carriers such as activated carbon fiber [32], activated carbon honeycomb [33], ZSM5 [34], have attracted a great deal of attention for their excellent catalytic performance on NO removal. Additionally, it has been reported that Mn-Ce mixed oxides exhibited excellent oxidative capacity attributed to its redox property, which was based on reversible adsorption/desorption cycles of lattice oxygen [35]. One thus expects Mn-Ce mixed oxides supported on columnar activated coke, which is commercial available for industrial desulfurization, to be a competitive catalyst/adsorbent for Hg^0 removal at low temperature and without the aid of HCl.

In this work, MnCe/AC catalysts/adsorbents were employed to remove Hg^0 in a wide reaction temperature range of 100–250 °C. The optimal reaction temperature and Mn-Ce mixed oxides loading values, as well as the effect of individual flue gas components were investigated. Besides, the mechanisms involved in Hg^0 adsorption and oxidation were identified. The ultimate goal is to develop an effective catalyst/adsorbent which is promising for industrial application in Hg^0 removal from low-rank coal combustion flue gas.

2. Experimental

2.1. Preparation of samples

All of activated cokes used in the experiment are commercial cokes from Inner Mongolia Kexing Carbon Industry Co., Ltd., which are in the form of cylinders with an average diameter of 6 mm and length of 10 mm. The samples were prepared by impregnation method, detail steps are as follows. Firstly, AC was washed with deionized water for several times and dried in an electric blast oven at 105 °C for 12 h. Secondly, different amount of cerium nitrate and manganese acetate were dissolved in deionized water to form mixed solution and a certain amount of AC was impregnated in the solution for 24 h. Thirdly, the mixtures were dried in an electric blast oven at 105 °C for 12 h and calcined in an electric tube furnace at 500 °C for 4 h under N_2 atmosphere. Finally, the samples were cooled to room temperature and then stored in a desiccator for further study. The mass ration of Mn/Ce was set as 1:1 in all MnCe/AC samples, which was demonstrated to be the optimal ration of MnO_x-CeO_2/ACH catalyst for NO removal [33]. Besides, the mass percentage of Mn-Ce mixed oxides of the MnCe/AC samples were 2%, 4%, 6%, 8%, 10%, respectively, which was denoted as MnCe*x*/AC, where x represents the MnCe percentage of the sample. In addition, for comparison, Mn/AC and Ce/AC were prepared with the same method mentioned above.

2.2. Characterization of samples

Brunauer–Emmett–Teller (BET) surface area of the samples was determined by N_2 adsorption with Micromeritics TristarII3020 analyzer (Micromeritics Instrument Crop., USA). Prior to BET measurements, all of the samples were degassed at 105 °C for 5 h.

X-ray diffraction (XRD) measurements were carried out on a Bruker D8-Advance X-ray diffraction device to examine the crystallinity and dispersivity of manganese and cerium species on the activated coke using CuKa radiation (λ = 0.1543 nm) in the range of 10–80° (2θ) with a step size of 0.02°.

X-ray photoelectron spectroscopy (XPS) analysis was carried out on a K-Alpha 1063X-ray photoelectron spectrometer (Thermo Fisher Scientific, USA) with an Al Ka X-ray source at room temperature. The observed spectra were adjusted with the C 1s binding energy (BE) value of 284.6 eV.

Temperature programmed desorption (TPD) analysis was conducted on an electric tube furnace SK-G06123K (Tianjin Zhonghuan Experiment Electric Furnace Co., Ltd., China). Before the TPD experiment, a certain amount of MnCe6/AC was first treated with a gas flow of Hg^0 balanced in N_2 and 6% O_2 at 190 °C for 12 h, and then the pretreated samples were heated at a constant heating rate of 5 °C/min to the last temperature of 600 °C.

2.3. Experimental setup and procedure

A fixed-bed experimental system was built so as to evaluate the performance of MnCe/AC samples on Hg^0 removal, as shown in Fig. 1. The test unite was consisted of a gas feed system, a Hg^0 vapor generating device, an electric tube furnace reactor, an on-line mercury analyzer and a data acquisition computer.

During each test, a certain amount of catalysts were laid in a quartz tube with an inner diameter of 52 mm and a length of 950 mm, which was placed horizontally in an electric tube furnace for the reaction temperature regulation. All individual flue gas components from cylinder gases were mixed in a gas mixing chamber, which was heated by a temperature controller. The flow rate of the each flue gas was accurately controlled by mass flow controllers and the total flow rate was set at 1 L/min, the mass of the samples used in each test was about 18 g, corresponding to a space velocity of around 5000 h^{-1}. The time for each test was 3 h. Hg^0 vapor was introduced into the gas mixing chamber using a certain amount of high-purity grade of N_2 (99.999%) from a Hg^0 permeation tube which was sealed in a U-shaped tube (placed in a water bath with a temperature of 65 °C).

Five sets of experiments were carried out, and the reaction conditions were summarized in Table 1. Set I experiment was designed to figure out the optimal loading value of Mn-Ce mixed oxides on activated coke and Set II was aimed at determining the optimal reaction temperature for Hg^0 removal over the optimal catalyst,

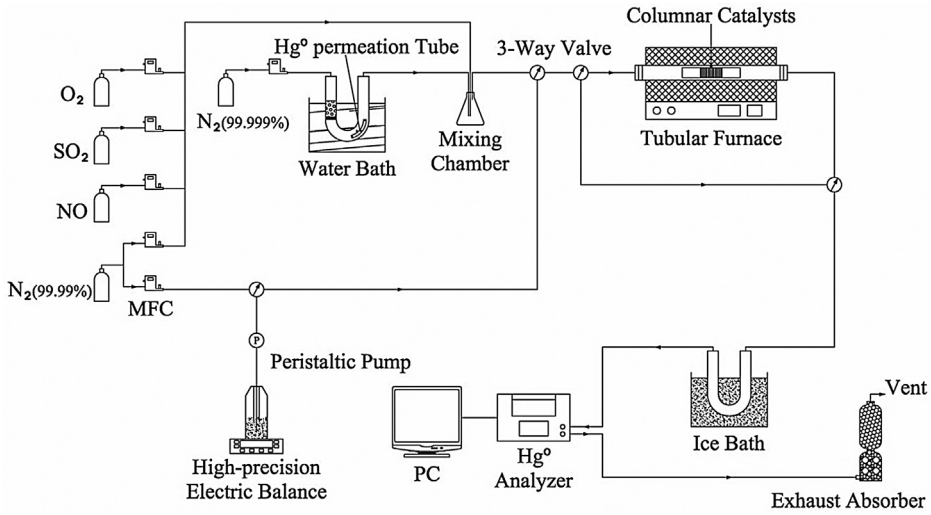

Fig. 1. Schematic diagram of experimental setup.

both of them were conducted under simple flue gas components. In set III, a comparative experiment between the performance of Mn6/AC, Ce6/AC and MnCe6/AC on Hg^0 removal was conducted to investigate the effect of active component and explore the possible reaction between MnO_x and CeO_2. In set IV, we tried to explore the roles of the individual flue gas components on Hg^0 removal, in addition, the activity of MnCe6/AC on Hg^0 removal under simulated flue gas components was evaluated. In set V, a Hg-TPD experiment was carried out to assist us in identifying the mechanism of Hg^0 removal over MnCe6/AC by determining the mercury species formed on the catalysts. In set VI, a test was conducted so as to explore whether HgO was absorbed on the surface of MnCe6/AC samples or desorbed from the samples into the outlet flue gas. In this set of experiment, a mercury conversion system was used to determine the concentration of Hg^{2+} in outlet flue gas. The detailed description of the mercury conversion system can be seen in our previous study [60]. During each experiment, the gas flow firstly bypassed the fix-bed reactor until a stable inlet concentration of Hg^0 (about 80 $\mu g/m^3$) was obtained. Then, the gas stream was introduced to pass through the catalyst for a certain period of time. At last, the gas flow bypassed the reactor again so as to verify the inlet concentration of Hg^0. The Hg^0 concentration was detected by a RA915M Mercury Analyzer (Lumex Co., Ltd., Russia), the detection limit of which is 2 ng/m^3 and can measure only the elemental mercury concentration according to Zeeman absorption spectrometry. All of pipes in the experiment were heated by temperature controllers at a constant temperature of 100 °C to avoid Hg^0 condensation and adsorption. The definition of Hg^0 removal efficiency (E_{rem}) was given below:

$$E_{rem}(\%) = \frac{\Delta Hg^0}{[Hg^0]_{in}} = \frac{[Hg^0]_{in} - [Hg^0]_{out}}{[Hg^0]_{in}} \times 100\% \quad (1)$$

$[Hg^0]_{in}$: inlet Hg^0 concentration of the reactor ($\mu g/m^3$); $[Hg^0]_{out}$: outlet Hg^0 concentration ($\mu g/m^3$).

Prior to testing the Hg^0 removal efficiency over the samples, blank tests were performed to eliminate any interference from the experimental system. The results showed negligible difference between the inlet and outlet data, which proved the inertness of the experimental system. It is known to all that experimental errors are inevitable. Therefore, E_{rem} is the average of three or more replicates under the same reaction conditions.

3. Results and discussion

3.1. Characterization of samples

3.1.1. BET analysis

The specific surface area, pore volume, and pore diameter of the samples The physical properties including BET surface area, pore volume and average pore diameter of virgin AC and impregnated AC are shown in Table 2. Taken as a whole, the AC impregnated with Mn-Ce mixed oxides possess higher BET surface area and pore volume than untreated AC to a certain extent, except for MnCe10/AC. Similar trend was found in other literatures [30,36]. In the process of impregnation and calcination, some new pores might be generated due to the reaction between AC and active components, which account for the higher BET surface area of impregnated AC compared with virgin AC. Nevertheless, it is easy to find that the BET surface area and total pore volume of impregnated AC decreased with the increase of Mn-Ce mixed oxides loading value, which can be resulted from the deposition of MnO_x and CeO_2 particles in some pores of AC [37].

3.1.2. XRD analysis

The XRD patterns of virgin AC and other Mn-Ce loaded AC samples are shown in Fig. 2. As to virgin AC, two strong diffraction peaks attributed to AC were detected at 26.66° and 44.58°. Nevertheless, the intensity of the two peaks obviously decreased with

Table 1
The experimental reaction conditions.

Experiment	Catalysts	Flue gas components	Temperature (°C)
Set I	Virgin AC, 2–10%MnCe/AC	$N_2 + 6\%O_2 + Hg^0$	190
Set II	MnCe6/AC	$N_2 + 6\%O_2 + Hg^0$	100, 130, 160, 190, 220, 250
Set III	Mn6/AC, Ce6/AC, MnCe6/AC	$N_2 + 6\%O_2 + Hg^0$	The optimal temperature
Set IV	MnCe6/AC	$N_2/(N_2 + O_2)$ + individual flue gas (NO, SO_2, H_2O)	The optimal temperature
Set V	MnCe6/AC treated with Hg^0	N_2	0–600
Set VI	MnCe6/AC	$N_2 + 6\%O_2 + Hg^0$	190

Table 2
The specific surface area, pore volume, and pore diameter of the samples.

Catalysts	BET surface area (m^2/g)	Total pore volume (cm^3/g)	Average pore diameter (nm)
Virgin AC	366.07	0.169	1.854
MnCe2/AC	468.39	0.220	1.879
MnCe4/AC	405.81	0.186	1.837
MnCe6/AC	382.86	0.177	1.848
MnCe8/AC	378.24	0.174	1.839
MnCe10/AC	280.14	0.132	1.887

the increase of Mn-Ce mixed oxides content, what's more, when the Mn-Ce mixed oxides loading values reached 8% and 10%, the peaks due to AC even disappeared, indicating that MnO_x and CeO_2 interacted with AC intensely in theses samples. For MnCe8/AC and MnCe10/AC, three peaks belong to CeO_2 were detected at $2\theta = 27.88^\circ$, 46.98° and 56.14°, respectively [31]. In contrast, no obvious peak of CeO_2 was observed when the Mn-Ce mixed oxides content is below 8%, this can be explained by the monolayer dispersion theory [38], which proposed that the metal oxide whether in a crystalline phase or not depends on the oxide content and its threshold value. What interest us is that no apparent peak due to manganese oxides was observed among all samples although manganese was surely involved in the MnCe/AC samples, which is in accord with the XRD result of Mn-Ce/Ti catalyst researched by Li [12]. This indicated that manganese oxides existed as an amorphous phase or highly dispersed on the surface of AC, which can promote the catalytic oxidation activity efficiently [39].

3.1.3. XPS analysis

To determine the chemical state and the relative portion of the main elements on the surface of different samples, Mn6/AC, Ce6/AC, fresh MnCe6/AC and used MnCe6/AC were investigated by XPS technique. The XPS spectra of Mn 2p, O 1s, Ce 3d for the fresh and used samples were fitted by Gaussian model and the results are shown in Figs. 3–5. The relative content of Mn^{4+}/Mn^{3+} over different samples was calculated from the sum of areas of the Mn^{4+} to the sum of areas of the Mn^{3+}, and the relative content of Ce^{4+}/Ce^{3+} was calculated by the similar way.

As for O 1s, three types of oxygen were observed on the catalysts, the peaks at low binding energy could be regarded as lattice oxygen (denoted as O_α), the binding energy peak at 531.0–531.7 eV is attributed to chemisorbed oxygen and OH groups (denoted as O_β), and the peak at 532.7–533.5 eV was reported to exist in molecular water (denoted as O_γ) [40,41]. In this study, the concentration of

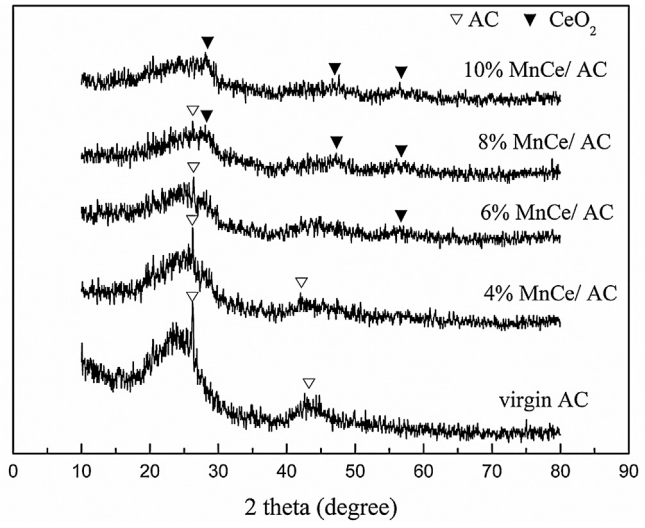

Fig. 2. XRD patterns of virgin AC and MnCe/AC samples.

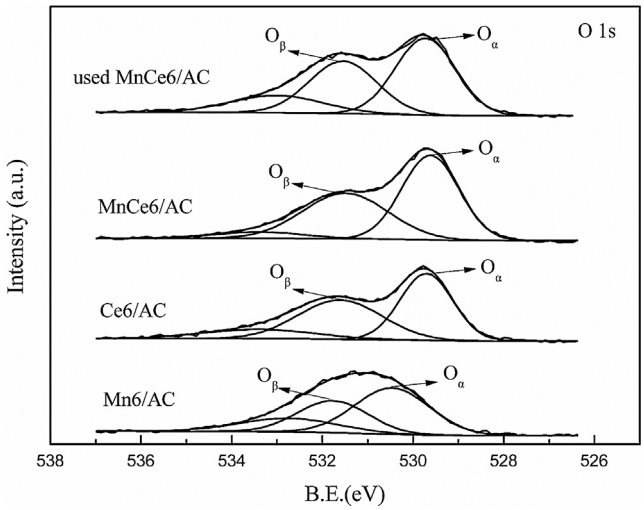

Fig. 3. XPS spectra of O 1s for Mn6/AC, Ce6/AC, MnCe6/AC and used MnCe6/AC.

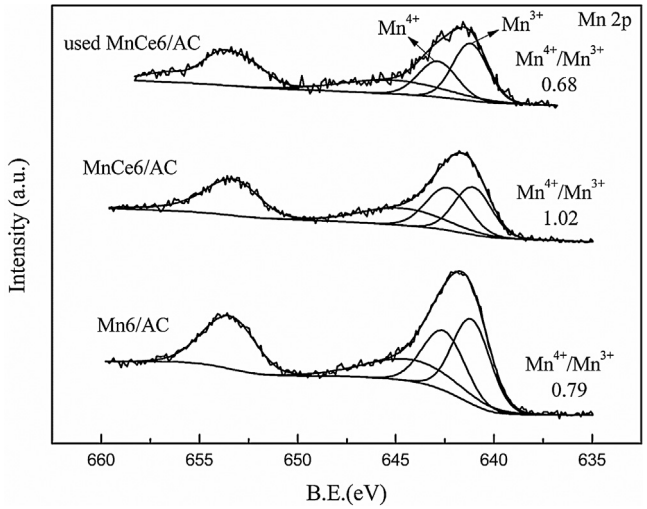

Fig. 4. XPS spectra of Mn 2p for Mn6/AC, MnCe6/AC and used MnCe6/AC.

O_α, O_β and O_γ on the samples were calculated by $O_\alpha/(O_\alpha + O_\beta + O_\gamma)$, $O_\beta/(O_\alpha + O_\beta + O_\gamma)$, and $O_\gamma/(O_\alpha + O_\beta + O_\gamma)$, respectively. As illustrated by Table 3, the O_β concentration of MnCe6/AC increased by around 10% in comparison with that of Mn6/AC, indicating that the

Table 3
The concentrations of different type of oxygen (O_α, O_β, O_γ) in Mn6/AC, Ce6/AC, MnCe6/AC and used MnCe6/AC.

Samples	O_α	O_β	O_γ
Mn6/AC	52.11%	33.15%	14.74%
Ce6/AC	44.67%	41.94%	13.38%
MnCe6/AC	52.18%	42.15%	5.67%
Used MnCe6/AC	47.58%	36.22%	16.20%

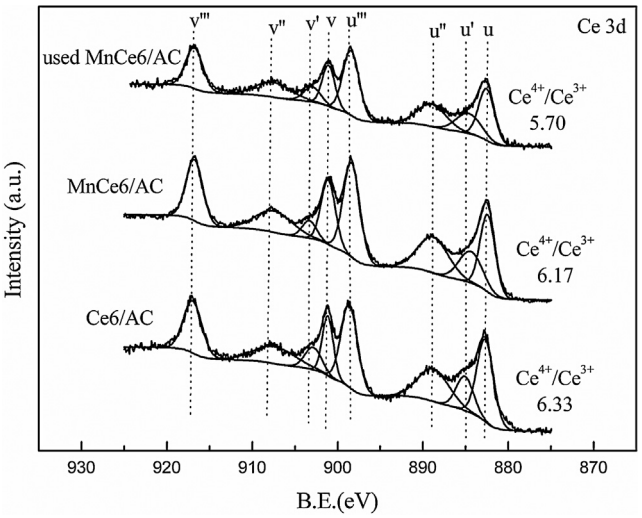

Fig. 5. XPS spectra of Ce 3d for Ce6/AC, MnCe6/AC and used MnCe6/AC.

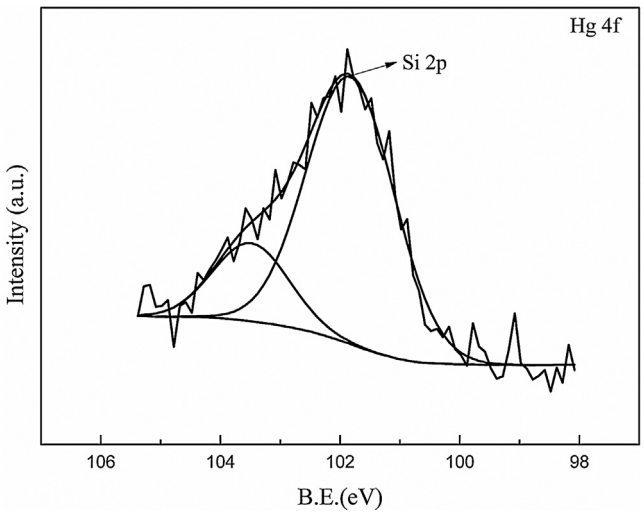

Fig. 6. XPS spectra of Hg 4f for used MnCe6/AC.

combination of MnO_x and CeO_2 resulted in more chemisorbed oxygen and oxygen vacancies, which is helpful to enhance the mobility of lattice oxygen, and improve the catalytic oxidation activity [42]. Wu et al. [43] also found that the concentration of chemisorbed oxygen on the catalysts was increased obviously by adding CeO_2 to MnO_x/TiO_2. Therefore, the relative high content of chemisorbed oxygen and oxygen vacancies on the surface of MnCe6/AC was at least partly responsible for its excellent performance on Hg^0 removal. Meanwhile, it is interesting to note that more lattice oxygen existed on MnCe6/AC than that on Ce6/AC, which might be benefit from abundant lattice oxygen contained in MnO_x. Moreover, compared with the fresh MnCe6/AC, the content of lattice oxygen on used MnCe6/AC decreased from 52.18% to 47.58% and the content of chemisorbed oxygen or OH groups decreased from 42.15% to 36.22%, in this regard, we can inferred that both lattice oxygen and chemisorbed oxygen or OH groups took part in the reaction of Hg^0 oxidation.

Similar as other Mn containing catalysts [40,20,44], Mn 2p region of catalysts in this study included a spin-orbit doublet with Mn 2p3/2 owing a binding energy of around 641.8 eV and Mn 2p1/2 with a binding energy of 653.4 eV. As shown in Fig. 4, Mn 2p3/2 can be fitted into three peaks, the peaks at 641.1 and 642.5 eV are attributed to Mn^{3+} and Mn^{4+}, respectively. This was in good agreement with some other studies [45,46]. Besides, the samples were calcined at 500 °C for 4 h in the process of catalysts preparation, which made the manganese oxides existed at the mixed states of Mn^{4+} and Mn^{3+} in the samples. As can be seen from Fig. 4, the portion of Mn^{4+} on MnCe6/AC increased compared to that on Mn6/AC, implying that some reactions took place when MnO_x and CeO_2 were combined, the possible reaction was as follows [47]:

$$2CeO_2 + Mn_2O_3 \rightarrow Ce_2O_3 + 2MnO_2 \quad (2)$$

Additionally, the ration of Mn^{4+}/Mn^{3+} decreased from 1.02 to 0.68 after the MnCe6/AC was used to remove Hg^0. This result indicated that MnO_2 on MnCe6/AC participated in Hg^0 oxidation reactions.

The XPS spectra of Ce 3d for different samples are presented in Fig. 5. Peaks denoted as u are attributed to Ce 3d3/2 spin-orbit states, while those denoted as v represent Ce 3d5/2 states. Furthermore, the u/v, u''/v'' and u'''/v''' doublets are due to Ce^{4+}, and u'/v' are assigned to Ce^{3+} [48,49]. It can be observed from Fig. 5 that cerium exists mainly in the form of Ce^{4+} oxidation state on the surface of both Ce6/AC and MnCe6/AC. However, it is worth noting that the portion of Ce^{3+} increased when the MnO_x and CeO_2 were combined together in this study. Ce^{3+} were reported to be able to create charge imbalance, more vacancies and unsaturated chemical bonds over the catalysts surface [50], thus increasing chemisorbed oxygen on the catalysts and improving the Hg^0 removal capacity, which can be verified by the XPS spectra of O 1s for Ce6/AC and MnCe6/AC. Besides, the ration of Ce^{4+}/Ce^{3+} decreased from 6.72 to 5.70 after the MnCe6/AC was used to remove Hg^0. It can be inferred from this result that CeO_2 contributed to Hg^0 removal in some way.

The XPS spectra of Hg 4f for used MnCe6/AC is shown in Fig. 6. An obvious peak at around 102.1 eV was attributed to Si 2p electron, for Si is the ingredient element of activated coke. Besides, a peak at about 103.8 eV was observed, which could be ascribed to HgO [51]. It is worth noting that no peak due to elemental mercury was found in spite of its existence was demonstrated by the TPD experiment. This may be owing to the low content of Hg^0 on the surface of the catalyst, which is much lower than the detection limit of XPS analysis.

3.2. Performance of the catalysts

3.2.1. Effect of loading value

The effect of Mn-Ce mixed oxides loading value on Hg^0 removal efficiency is shown in Fig. 7. Compared to virgin AC, MnCe/AC promoted mercury removal vastly, which indicated that AC, MnO_x and CeO_2 played a synergetic role in Hg^0 removal. As can be seen from Fig. 7, the mercury removal efficiency increased with the increase of Mn-Ce mixed oxides loading value when it was below 6%, and then decreased as the loading value further increased to 10%. From the above phenomena and aforementioned analysis of BET, it is obvious that the mercury removal efficiency was not consistent with the BET surface area of the samples, implying that physical adsorption played a certain role but not the dominant role in mercury removal over MnCe/AC. In the subsequent study, MnCe6/AC was chosen as the catalyst due to its best performance among all the samples.

3.2.2. Effect of active component

The performance of Mn6/AC, Ce6/AC and MnCe6/AC on mercury removal were evaluated under $N_2 + O_2 + Hg^0$ atmosphere at 190 °C, the results are shown in Fig. 8. The mercury removal efficiencies over Mn6/AC and Ce6/AC were 79.12% and 84.59%, respectively. However, MnCe6/AC obviously exhibited a higher mercury removal capacity than both of them, with a removal efficiency of 94.87%. These results demonstrated that MnO_x and CeO_2 reacted with each

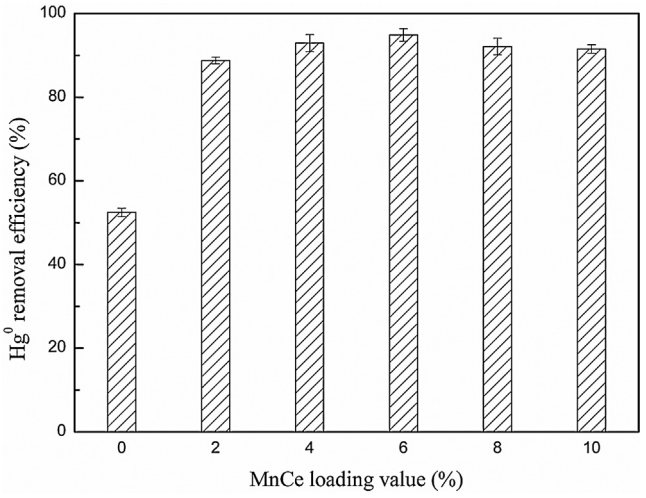

Fig. 7. Effects of Mn-Ce oxides loading values on Hg^0 removal efficiency. Reaction conditions: 6% O_2, ~80 μg/m^3 Hg^0, N_2 as balance. GHSV = 5000 h^{-1}, T = 190 °C, the reaction time for each test was 3 h.

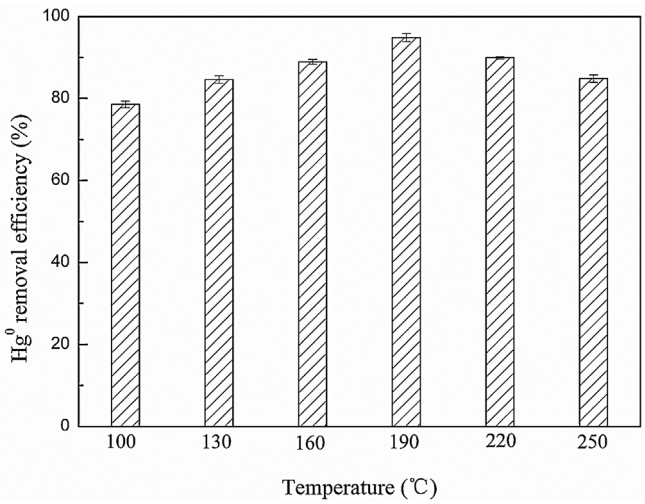

Fig. 9. Effects of reaction temperature on Hg^0 removal efficiency. Reaction conditions: 6% O_2, ~80 μg/m^3 Hg^0, N_2 as balance. GHSV = 5000 h^{-1}, T = 100 °C, 130 °C, 160 °C, 190 °C, 220 °C, 250 °C, the reaction time for each test was 3 h.

other and played a synergistic role in Hg^0 removal when they were combined. According to the analysis of XPS characterization of Mn6/AC, Ce6/AC and MnCe6/AC catalysts and another literature [47], the synergistic mechanism can be explained by the following reactions:

$$2MnO_2 \rightarrow Mn_2O_3 + O \quad (3)$$

$$2CeO_2 + Mn_2O_3 \rightarrow Ce_2O_3 + 2MnO_2 \quad (2)$$

$$2Ce_2O_3 + O_2 \rightarrow 4CeO_2 \quad (4)$$

The higher Hg^0 removal efficiency of MnCe6/AC than Mn6/AC and Ce6/AC might be related to the coexistence of MnO_2 and Mn_2O_3, CeO_2 and Ce_2O_3 [35]. The oxygen diffused from MnO_2 bulk to the surface of the catalyst and be the surface lattice oxygen, which was more active and easier to access. The bulk lattice oxygen vacancies of MnO_x were replenished by CeO_2, and CeO_2 was regenerated by adsorbing gas-phase O_2 from feed gas stream.

3.2.3. Effect of reaction temperature

Hg^0 removal efficiency over MnCe6/AC under the conditions of basic set (6% O_2, ~80 μg/m^3 Hg^0 and balanced N_2) at different temperatures (100–250 °C) are shown in Fig. 9. It could be clearly seen that Hg^0 removal efficiency increased with the increase of temperature from 100 to 190 °C, and then decreased with the temperature further increased from 190 to 250 °C. This result was due to the fact that Mn-Ce mixed oxides are more active for Hg^0 oxidation at higher temperature. Nevertheless, the physical adsorption of Hg^0 by MnCe6/AC was inhibited at higher temperature. Therefore, it can be concluded that Hg^0 removal over MnC6/AC sorbents/catalysts were decided by the combination of Hg^0 adsorption and catalytic oxidation. In this study, the optimal reaction temperature was 190 °C.

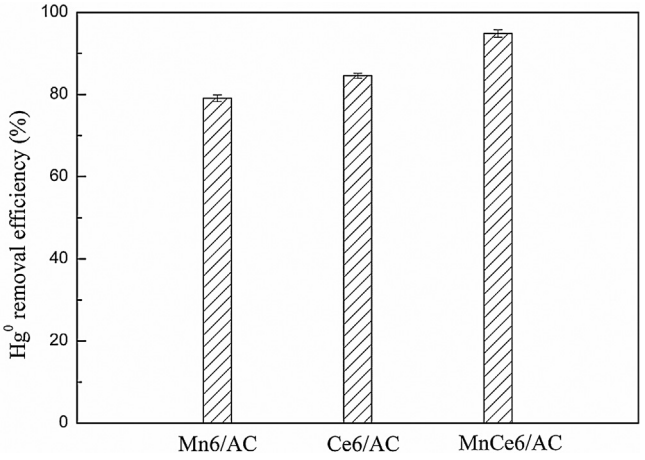

Fig. 8. Effects of active components on Hg^0 removal efficiency. Reaction conditions: 6% O_2, ~80 μg/m^3 Hg^0, N_2 as balance. GHSV = 5000 h^{-1}, T = 190 °C, the reaction time for each test was 3 h.

3.3. Effect of individual flue gas components

3.3.1. Effect of O_2

The mercury removal efficiency over MnCe6/AC at 190 °C under pure N_2 was observed to be about 80%, as shown in Fig. 10. The relative high mercury removal efficiency under pure N_2 was due to the abundance of surface oxygen (including chemisorbed oxygen and lattice oxygen) on MnCe6/AC and the relative strong adsorption capacity of activated coke, which can be verified by the analysis of

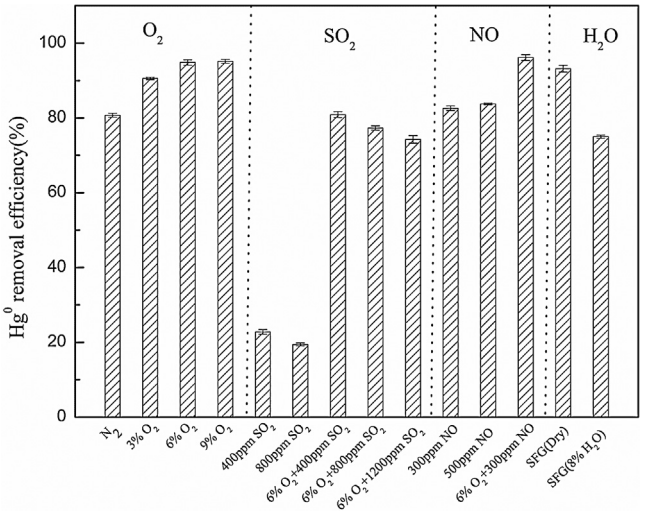

Fig. 10. Effects of individual flue gas components on Hg^0 removal efficiency. Reaction conditions: GHSV = 5000 h^{-1}, T = 190 °C, the reaction time for each test was 3 h.

the XPS spectra of O1s for MnCe6/AC catalysts/adsorbents in Section 3.1.3 and the mercury removal efficiency over virgin AC which can be observed from Fig. 7. When 3% O_2 was added to the pure N_2 gas stream, the mercury removal efficiency increased from 80% to around 90%, and further increased to about 95% with the concentration of O_2 came to 6%. Gas-phase O_2 would replenish the lattice and chemisorbed oxygen [52] which has been consumed in the process of Hg^0 oxidation reaction, thus displaying a promotional effect on Hg^0 removal. It should be noted that the mercury removal efficiency remained almost the same even when the concentration of O_2 increased to 9%, indicating that, for the MnCe6/AC catalyst, 6% O_2 was sufficient to replenish the consumed surface oxygen, and then sustained the Hg^0 oxidation.

3.3.2. Effect of SO_2

Inconclusive effects of SO_2 on mercury removal have been found over different catalysts and adsorbents, including inhibitive [53], promotional [23] and insignificant effects [54]. In this study, it was observed that SO_2 suppressed mercury removal seriously under pure N_2 atmosphere, as shown in Fig. 10, when 400 ppm SO_2 was added to the pure N_2 gas flow, mercury removal efficiency decreased from 80.74% to 22.79% and further decreased to 19.41% with the concentration of SO_2 increased to 800 ppm. Two possible reasons were responsible for this result, on one hand, SO_2 compete with Hg^0 for active sites on the MnCe6/AC [55], thus inhibiting the Hg^0 adsorption, which is necessary for the Hg^0 oxidation over MnCe6/AC. On the other hand, the adsorbed SO_2 reacted with the surface oxygen of the catalyst [56], thus hindering the reaction between Hg^0 and surface oxygen. It could be inferred that the consumption of surface oxygen by SO_2 was the dominant factor since an obvious reduction of inhibitive effect was observed when gas-phase O_2 was added to the gas flow in this work, as shown in Fig. 10. The mercury removal efficiency increased from 22.79% to 80.88% when 6% O_2 was added to the gas flow, the reason responsible for it was that, for one thing, gas-phase O_2 would replenish the consumed surface oxygen, for the other, SO_2 may directly react with O_2 over the catalyst [57] and spare the lattice oxygen to oxidize the adsorbed Hg^0.

3.3.3. Effect of NO

Compared with pure N_2 atmosphere, an addition of 300 ppm NO exhibited a very slight promotional effect, namely around 2%, on mercury removal. Further increased the concentration of NO to 500 ppm caused no significant variation. It has been reported that, in the absence of O_2, NO would be weakly adsorbed on the surface of the metal oxide catalysts [54,55], and then a part of it would react with the surface oxygen to generate NO_2 and NO^+ species [56]. In this regard, on one side, the surface oxygen of the catalysts, which was responsible for Hg^0 oxidation, was consumed by NO when it was added to the pure N_2 gas flow. On the other side, NO_2, as the production of reaction between NO and the surface oxygen, has been reported to be active for Hg^0 oxidation [55]. Therefore, a very light promotional effect of NO on mercury removal observed in this study was attributed to the combination influence of the above stated two aspects. Fig. 10 revealed that, in the presence of 6% O_2 and 300 ppm NO, a significant higher mercury removal efficiency was obtained than in the presence of NO alone, this might be due to the replenishment of the consumed surface oxygen by the gas-phase O_2.

3.3.4. Effect of H_2O

Water vapor, as an unavoidable component of coal-fired flue gas, has been found to cause a negative impact on mercury removal over various metal oxide catalysts [23,54,57], and the same phenomenon was observed in this work. As revealed in Fig. 10, an addition of 8% water vapor into dry simulated flue gas led to about 18% declination of mercury removal efficiency. Two possible reasons were responsible for it, firstly, water vapor competed with Hg^0 for active sites and thus inhibiting the Hg^0 adsorption [54]. Additionally, the adsorbed water vapor may react with SO_3 and Mn-Ce oxides to form sulfate, which would cover the surface of the catalysts and affect the Hg^0 oxidation by deactivating the catalyst to a certain extent [31].

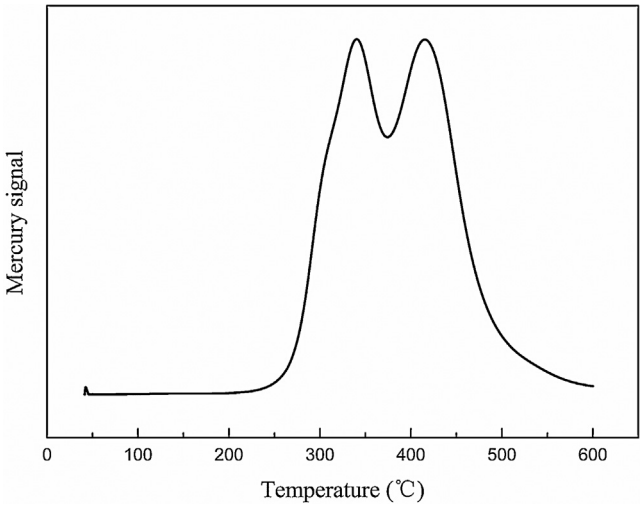

Fig. 11. Hg-TPD profile of pretreated MnCe6/AC.

3.4. Identification of Hg^0 removal mechanism

Fig. 11 displays the Hg-TPD profile of pretreated MnCe6/AC catalysts. It can be seen that one small mercury desorption peak appeared at about 40 °C and two obvious peaks appeared at around 340 °C and 425 °C, respectively. On the basis of the decomposition temperatures for different mercury compounds and some previous literatures [58,59], the small peak is assigned to physical adsorption Hg^0 and the obvious peaks were due to HgO, moreover, it can be concluded from the figure that HgO was the dominant species present on the used MnCe6/AC catalysts, this is consistent with the result of XPS spectra for Hg 4f.

The experiment result of set VI showed that the concentration of total mercury and elemental mercury in the outlet flue gas was nearly the same to each other, which indicated that the formed HgO was adsorbed on the surface of the MnCe6/AC samples. Similar conclusions had been drawn in some other studies [61,62].

According to the above discussion of the experimental and characterization results, the mechanisms of Hg^0 removal over MnCe6/AC sorbents/catalysts can be explained by the combination of adsorption and oxidation, furthermore, both the lattice oxygen and OH groups on MnCe6/AC made a contribution to Hg^0 oxidation. At first, Hg^0 was physically adsorbed on the active sites of the MnCe6/AC, and then parts of adsorbed Hg^0 reacted with the lattice oxygen which was abstracted from MnO_2 to form HgO. The consumed lattice oxygen of MnO_2 can be replenished by CeO_2, and the Ce^{3+} could be oxidized by gas-phase O_2, thus sustaining the Hg^0 oxidation process. Additionally, parts of adsorbed Hg^0 reacted with chemisorbed oxygen or OH groups to form HgO. The main reactions are as follows:

$$Hg^0(g) \rightarrow Hg^0(ad) \quad (5)$$

$$Hg^0(ad) + 2MnO_2 \rightarrow HgO(ad) + Mn_2O_3 \quad (6)$$

$$2CeO_2 + Mn_2O_3 \rightarrow Ce_2O_3 + 2MnO_2 \quad (2)$$

$$2Ce_2O_3 + O_2 \rightarrow 4CeO_2 \quad (4)$$

4. Conclusions

In this study, Mn-Ce mixed oxides supported on commercial available activated cokes were prepared and applied to remove elemental mercury from flue gas without the assistance of HCl. In comparison to virgin AC, Mn/AC and Ce/AC, MnCe/AC showed the highest capacity for Hg^0 removal, with the efficiency up to 94%. Results indicated that the optimal Mn-Ce loading value and reaction temperature were 6% and 190 °C, respectively. Besides, the mercury removal efficiency was affected by flue gas components to some extent, thereinto, O_2 and NO were beneficial for Hg^0 removal. SO_2 showed an obvious inhibitory effect on Hg^0 removal when in the absence of O_2. However, this inhibitory effect can be greatly reduced by adding 6% O_2 into the flue gas. What's more, water vapor had a negative impact on Hg^0 capture as well. Finally, the analysis of XPS and TPD indicated that the main species of mercury on used MnCe6/AC was HgO, and the Hg^0 oxidation over MnCe6/AC benefited from both lattice oxygen and chemisorbed oxygen or OH groups on the surface of MnCe6/AC.

This research provided some basic information for industrial application of MnCe/AC adsorbents and catalysts in low-rank coal-fired power plants. Considering the cost savings and convenience for air pollution control, the capacity of MnCe/AC for removing Hg^0 and NO simultaneously from flue gas will be investigated in the future. Moreover, the regeneration of used MnCe/AC will be studied as well.

Acknowledgements

The project is supported by the National Natural Science Foundation of China (51278177, 51478173), and the National High Technology Research and Development Program of China (863 Program, No. 2011AA060803).

References

[1] J.H. Pavlish, E.A. Sondreal, M.D. Mann, E.S. Olson, K.C. Galbreath, D.L. Laudal, S.A. Benson, Status review of mercury control options for coal-fired power plants, Fuel Process. Technol. 82 (2003) 89–165.
[2] T.D. Brown, D.N. Smith, R.A. Hargis, Mercury measurement and its control: what we know, have learned, and need to further investigate, J. Air Waste Manage. Assoc. 49 (1999) 628–640.
[3] Y. Wu, S.X. Wang, D.G. Streets, Trends in anthropogenic mercury emissions in China from 1995 to 2003, Environ. Sci. Technol. 40 (2006) 5312–5318.
[4] U.S. Environmental Protection Agency, Air Toxics Standards for Utilities, 2015, http://www.epa.gov/airquality/powerplanttoxics/actions.html (accessed 12.21.11).
[5] K.C. Galbreath, C.J. Zygarlicke, Mercury transformations in coal combustion flue gas, Fuel Process. Technol. 65–66 (2000) 289–310.
[6] Y. Zhuang, J.S. Thompson, C.J. Zygarlicke, J.H. Pavlish, Development of a mercury transformation model in coal combustion flue gas, Environ. Sci. Technol. 38 (2004) 5803–5808.
[7] A. Stergaršek, M. Horvat, P. Frkal, S.R. Guevara, R. Kocjančič, Removal of Hg^0 in wet FGD by catalytic oxidation with air – a contribution to the development of a process chemical model, Fuel 107 (2013) 183–191.
[8] F. Scala, H. Clack, Mercury emissions from coal combustion: modeling and comparison of Hg capture in a fabric filter versus an electrostatic precipitator, J. Hazard. Mater. 152 (2008) 616–623.
[9] Y.J. Wang, Y.F. Duan, L.G. Yang, C.S. Zhao, X.L. Shen, M.Y. Zhang, Y.Q. Zhuo, C.H. Chen, Experimental study on mercury transformation and removal in coal-fired boiler flue gases, Fuel Process. Technol. 90 (2009) 643–651.
[10] Y. Liu, Y.J. Wang, H.Q. Wang, Z.B. Wu, Catalytic oxidation of gas-phase mercury over Co/TiO_2 catalysts prepared by sol–gel method, Catal. Commun. 12 (2011) 1291–1294.
[11] P.Y. Wang, S. Su, J. Xiang, F. Cao, L.S. Sun, S. Hu, S.Y. Lei, Catalytic oxidation of Hg^0 by $CuO\text{-}MnO_2\text{-}Fe_2O_3/\gamma\text{-}Al_2O_3$ catalyst, Chem. Eng. J. 225 (2013) 68–75.
[12] H. Li, C.Y. Wu, Y. Li, J. Zhang, Superior activity of $MnO_x\text{–}CeO_2/TiO_2$ catalyst for catalytic oxidation of elemental mercury at low flue gas temperatures, Appl. Catal. B: Environ. 111–112 (2012) 381–388.
[13] S. Sjostrom, M. Durham, C. Jean Bustard, C. Martin, Activated carbon injection for mercury control: overview, Fuel 89 (2010) 1320–1322.
[14] R.D. Vidic, D.P. Siler, Vapor-phase elemental mercury adsorption by activated carbon impregnated with chlorine and chelating agents, Carbon 39 (2001) 3–14.
[15] J. Liu, M.A. Cheney, F. Wu, M. Li, Effects of chemical functional groups on elemental mercury adsorption on carbonaceous surfaces, J. Hazard. Mater. 186 (2011) 108–113.
[16] F. Scala, Modeling mercury capture in coal-fired power plant flue gas, Ind. Eng. Chem. Res. 43 (2004) 2575–2589.
[17] A.P. Jones, J.W. Hoffmann, D.N. Smith, T.J. Feeley, J.T. Murphy, DOE/NETL's phase II mercury control technology field testing program: preliminary economic analysis of activated carbon injection, Environ. Sci. Technol. 41 (2007) 1365–1371.
[18] S.J. Yang, Y.F. Guo, N.Q. Yan, D.Q. Wu, H.P. He, Z. Qu, J.P. Jia, Elemental mercury capture from flue gas by magnetic Mn–Fe spinel: effect of chemical heterogeneity, Ind. Eng. Chem. Res. 50 (2011) 9650–9656.
[19] H.Q. Yang, Z.H. Xu, M.H. Fan, A.E. Bland, R.R. Judkins, Adsorbents for capturing mercury in coal-fired boiler flue gas, J. Hazard. Mater. 146 (2007) 1–11.
[20] S.H. Qiao, J. Chen, J.F. Li, Z. Qu, P. Liu, N.Q. Yan, J.P. Jia, Adsorption and catalytic oxidation of gaseous elemental mercury in flue gas over MnO_x/alumina, Ind. Eng. Chem. Res. 48 (2009) 3317–3322.
[21] H.L. Li, C.Y. Wu, Y. Li, J.Y. Zhang, $CeO_2\text{-}TiO_2$ catalysts for catalytic oxidation of elemental mercury in low-rank coal combustion flue gas, Environ. Sci. Technol. 45 (2011) 7394–7400.
[22] W.Q. Xu, H.R. Wang, X. Zhou, T.Y. Zhu, CuO/TiO_2 catalysts for gas-phase Hg^0 catalytic oxidation, Chem. Eng. J. 243 (2014) 380–385.
[23] Q. Wan, L. Duan, K.B. He, J.H. Li, Removal of gaseous elemental mercury over a $CeO_2\text{-}WO_3/TiO_2$ nanocomposite in simulated coal-fired flue gas, Chem. Eng. J. 170 (2011) 512–517.
[24] H.L. Li, C.Y. Wu, Y. Li, J.Y. Zhang, Oxidation and capture of elemental mercury over $SiO_2\text{-}TiO_2\text{-}V_2O_5$ catalysts in simulated low-rank coal combustion flue gas, Chem. Eng. J. 169 (2011) 186–193.
[25] W. Gao, Q.C. Liu, C.Y. Wu, H.L. Li, Y. Li, J. Yang, G.F. Wu, Kinetics of mercury oxidation in the presence of hydrochloric acid and oxygen over a commercial SCR catalyst, Chem. Eng. J. 220 (2013) 53–60.
[26] K. Tsuji, I. Shiraishi, Combined desulfurization, denitrification and reduction of air toxics using activated coke: 1. Activity of activated coke, Fuel 75 (1997) 549–553.
[27] K. Tsuji, I. Shiraishi, Combined desulfurization, denitrification and reduction of air toxics using activated coke: 2. Process applications and performance of activated coke, Fuel 76 (1997) 555–560.
[28] D.G. Olson, K. Tsuji, I. Shiraishi, The reduction of gas phase air toxics from combustion and incineration sources using the MET-Mitsui-BF activated coke process, Fuel Process. Technol. 65–66 (2000) 393–405.
[29] J.W. Wang, J.L. Yang, Z.Y. Liu, Gas-phase elemental mercury capture by a V_2O_5/AC catalyst, Fuel Process. Technol. 91 (2010) 676–680.
[30] X.Y. Hua, J.S. Zhou, Q.K. Li, Z.Y. Luo, K.F. Cen, Gas-phase elemental mercury removal by CeO_2 impregnated activated coke, Energy Fuels 24 (2010) 5426–5431.
[31] S.S. Tao, C.T. Li, X.P. Fan, G.M. Zeng, P. Lu, X. Zhang, Q.B. Wen, W.W. Zhao, D.Q. Luo, C.Z. Fan, Activated coke impregnated with cerium chloride used for elemental mercury removal from simulated flue gas, Chem. Eng. J. 210 (2012) 547–556.
[32] B.X. Shen, T. Liu, N. Zhao, J. Ma, X.C. Hao, Research of catalytic performance over transition metal modified $MnO_x\text{-}CeO_x$/ACF catalysts, Adv. Mater. Res. 383–390 (2012) 1945–1950.
[33] Y.L. Wang, C.Z. Ge, L. Zhan, C. Li, W.M. Qiao, L.C. Ling, $MnO_x\text{-}CeO_2$/activated carbon honeycomb catalyst for selective catalytic reduction of NO with NH_3 at low temperatures, Ind. Eng. Chem. Res. 51 (2012) 11667–11673.
[34] G. Carja, Y. Kameshima, K. Okada, C.D. Madhusoodana, Mn-Ce/ZSM5 as a new superior catalyst for NO reduction with NH_3, Appl. Catal. B: Environ. 73 (2007) 60–64.
[35] G.S. Qi, R.T. Yang, R. Chang, $MnO_x\text{-}CeO_2$ mixed oxides prepared by co-precipitation for selective catalytic reduction of NO with NH_3 at low temperatures, Appl. Catal. B: Environ. 51 (2004) 93–106.
[36] L.H. Tian, C.T. Li, Q. Li, G.M. Zeng, Z. Gao, S.H. Li, X.P. Fan, Removal of elemental mercury by activated carbon impregnated with CeO_2, Fuel 88 (2009) 1687–1691.
[37] J.C. Serrano-Ruiz, E.V. Ramos-Fernández, J. Silvestre-Albero, A. Sepúlveda-Escribano, F. Rodríguez-Reinoso, Preparation and characterization of CeO_2 highly dispersed on activated carbon, Mater. Res. Bull. 43 (2008) 1850–1857.
[38] Y.Ch. Xie, Y.Q. Tang, Spontaneous monolayer dispersion of oxides and salts onto surfaces of supports: applications to heterogeneous catalysis, Adv. Catal. 37 (17) (1990) 1–43.
[39] Z.B. Wu, B.Q. Jiang, Y. Liu, Effect of transition metals addition on the catalyst of manganese/titania for low-temperature selective catalytic reduction of nitric oxide with ammonia, Appl. Catal. B: Environ. 79 (2008) 347–355.
[40] M. Kang, E.D. Park, J.M. Kim, J.E. Yie, Manganese oxide catalysts for NO_x reduction with NH_3 at low temperatures, Appl. Catal. A 327 (2007) 261–269.
[41] J.C. Dupin, D. Gonbeau, P. Vinatier, A. Levasseur, Systematic XPS studies of metal oxides, hydroxides and peroxides, Phys. Chem. Chem. Phys. 2 (2000) 1319–1324.
[42] H.Y. Chen, A. Sayari, A. Adnot, F. Larachi, Composition-activity effects of Mn-Ce-O composites on phenol catalytic wet oxidation, Appl. Catal. B: Environ. 32 (2001) 195–204.
[43] Z.B. Wu, R.B. Jin, Y. Liu, H.Q. Wang, Ceria modified MnO_x/TiO_2 as a superior catalyst for NO reduction with NH_3 at low-temperature, Catal. Commun. 9 (2008) 2217–2220.

[44] S.M. Lee, K.H. Park, S.C. Hong, MnO_x/CeO_2-TiO_2 mixed oxide catalysts for the selective catalytic reduction of NO with NH_3 at low temperature, Chem. Eng. J. 195–196 (195) (2012) 323–330.
[45] B. Thirupathi, P.G. Smirniotis, Nickel-doped Mn/TiO_2 as an efficient catalyst for the low-temperature SCR of NO with NH_3: catalytic evaluation and characterizations, J. Catal. 288 (2012) 74–83.
[46] Y.F. Guo, N.Q. Yan, S.J. Yang, P. Liu, J. Wang, Z. Qu, J.P. Jia, Conversion of elemental mercury with a novel membrance catalytic system at low temperature, J. Hazard. Mater. 213–214 (2012) 62–70.
[47] Z.Y. Ding, L.X. Li, D. Wade, E.F. Gloyna, Supercritical water oxidation of NH_3 over a MnO_2/CeO_2 catalyst, Ind. Eng. Chem. Res. 37 (1998) 1707–1716.
[48] Z.Q. Zou, M. Meng, Y.Q. Zha, Surfactant-assisted synthesis, characterizations, and catalytic oxidation mechanisms of the mesoporous MnO_x-CeO_2 and Pd/MnO_x-CeO_2 catalysts used for CO and C_3H_8 oxidation, J. Phys. Chem. C 114 (2010) 468–477.
[49] M. Romeo, K. Bak, J.E.L. Fallah, F. Le Normand, L. Hilaire, XPS study of the reduction of cerium dioxide, Surf. Interface Anal. 20 (1993) 508–512.
[50] S. Yang, W. Zhu, Z. Jiang, Z. Chen, J. Wang, The surface properties and the activities in catalytic wet air oxidation over CeO_2-TiO_2 catalysts, Appl. Surf. Sci. 252 (2006) 8499–8505.
[51] J. He, G.K. Reddy, S.W. Thiel, P.G. Smirniotis, N.G. Pinto, Ceria-modified manganese oxide/titania materials for removal of elemental and oxidized mercury from flue gas, J. Phys. Chem. C 115 (2011) 24300–24309.
[52] A. Bueno-López, K. Krishna, M. Makkee, J.A. Moulijn, Enhanced soot oxidation by lattice oxygen via La^{3+}-doped CeO_2, J. Catal. 230 (2005) 237–248.
[53] X.Y. Wen, C.T. Li, X.P. Fan, H.L. Gao, W. Zhang, L. Chen, G.M. Zeng, Y.P. Zhao, Experimental study of gaseous elemental mercury removal with CeO_2/γ-Al_2O_3, Energy Fuels 25 (2011) 2939–2944.
[54] Y. Li, P.D. Murphy, C.Y. Wu, K.W. Powers, J.J. Bonzongo, Development of silica/vanadia/titania catalysts for removal of elemental mercury from coal-combustion flue gas, Environ. Sci. Technol. 42 (2008) 5304–5309.
[55] G.S. Qi, R.T. Yang, Characterization and FTIR studies of MnO_x-CeO_2 catalyst for low-temperature selective catalytic reduction of NO with NH_3, J. Phys. Chem. B 108 (2004) 15738–15747.
[56] Y.N. Shi, S. Chen, H. Sun, Y. Shu, X. Quan, Low-temperature selective catalytic reduction of NO with NH_3 over MnCe oxides supported on TiO_2 and Al_2O_3: a comparative study, Catal. Commun. 12 (2013) 10–13.
[57] X.P. Fan, C.T. Li, G.M. Zeng, X. Zhang, S.S. Tao, P. Lu, Y. Tan, Q.D. Luo, Hg^0 removal from simulated flue gas over CeO_2/HZSM-5, Energy Fuels 26 (2012) 2082–2089.
[58] P.Y. Wang, S. Hu, J. Xiang, S. Su, L.S. Sun, F. Cao, X. Xiao, A.C. Zhang, Analysis of mercury species over CuO-MnO_2-Fe_2O_3/γ-Al_2O_3 catalysts by thermal desorption, Proc. Combust. Inst. (2015), http://dx.doi.org/10.1016/j.proci.2014.06.054.
[59] M.A. Lopez-Anton, Y. Yang, R. Perry, M.M. Maroto-Valer, Analysis of mercury species present during coal combustion by thermal desorption, Fuel 89 (2010) 629–634.
[60] J.F. Ma, C.T. Li, L.K. Zhao, J. Zhang, J.K. Song, G.M. Zeng, X.N. Zhang, Y.E. Xie, Study on removal of elemental mercury from simulated flue gas over activated coke treated by acid, Appl. Surf. Sci. 329 (2015) 292–300.
[61] W.Q. Xu, H.R. Wang, T.Y. Zhu, J.Y. Kuang, P.F. Jing, Mercury removal from coal combustion flue gas by modified fly ash, J. Environ. Sci. 25 (2013) 393–398.
[62] L.L. Xing, Y.L. Xu, Q. Zhong, Mn and Fe modified fly ash as a superior catalyst for elemental mercury capture under air conditions, Energy Fuels 26 (2012) 4903–4909.